Dilute gas Couette flow: Theory and molecular dynamics simulation

Dino Risso*
Departamento de Física, Facultad de Ciencias, Universidad del Bío-Bío, Casilla 1202, Concepción, Chile

Patricio Cordero†
Departamento de Física, Facultad de Ciencias Físicas y Matemáticas, Universidad de Chile, Casilla 487, Santiago 3, Chile

(Received 3 September 1996; revised manuscript received 26 December 1996)

Explicit analytic nonlinear laws of heat transport and of viscous flow are derived from Grad's approximate solution of Boltzmann's equation and they are shown to describe quite well the observations made in molecular dynamics simulations. With this aim a planar Couette flow is studied analytically and by means of microscopic molecular dynamics techniques for the case of a bidimensional gas of hard disks. The fluid develops a nonuniform temperature profile, shows a non-Newtonian behavior, and there is a heat current which obeys Fourier's law with a tensorial shear rate-dependent thermal conductivity. [S1063-651X(97)07507-7]

PACS number(s): 05.20.Dd, 47.50.+d, 51.10.+y

I. INTRODUCTION

Transport in dilute systems far from equilibrium is not a simple hydrodynamic problem. Even though the Navier-Stokes equations are the main tool to study the hydrodynamic behavior of fluids, behind these equations is the basic assumption that changes in a fluid take place smoothly and slowly so that the system can be considered in a state of local thermodynamic equilibrium and the transport of momentum and energy in it is described by linear constitutive equations (Newton's and Fourier's laws) which relate the gradients of the standard hydrodynamic variables (*forces*) with the momentum and heat flux vectors. When the condition of smooth or slow variation is not fully satisfied the fluid behavior may deviate from the predictions of standard hydrodynamic calculations: the linear relation between the *forces* and the fluxes breaks down and the constitutive equations have to be extended beyond the linear regime.

Kinetic theory, on the other hand, gives a more fundamental theory but it has been well developed only for rather dilute systems where Boltzmann's (or Enskog's) equation can be justified. The fundamental equation is that of Liouville or equivalently the Bogoliubov-Born-Green-Kirkwood-Yvon (BBGKY) hierarchy of equations for partial distributions.

Within the range of validity of Boltzmann's equation, the challenge is to find approximate solutions. Boltzmann's equation is complex enough that it is not obvious which approximate scheme should be used: (1) Chapman-Enskog method is perhaps the one most widely used, (2) the Bhatnagar-Groos-Krook (BGK) approximation that, in a way, linearizes Boltzmann's equation modifying the collision operator, or (3) Grad's momentum expansion method.

The Chapman-Enskog method is an expansion about equilibrium in gradients of the hydrodynamic fields: density n, velocity $\vec{v}$, and temperature T. The first order gives Euler's ideal hydrodynamics and the second order provides a version of Navier-Stokes equations with *linear transport equations* and explicit expressions for the transport coefficients [1,2]. The BGK approximation [3] deals with a kinetic equation where Boltzmann's collisional operator has been replaced by a simpler one $J[ff] \rightarrow n\nu\,(f_{\mathrm{eq}} - f)$ and it has been used to deal with the problem at stake as we comment below.

Grad's method [4] uses a self-consistent approach involving higher momenta and no gradients of them. In particular, Grad worked out in detail the case when the distribution function f is written in terms of n, $\vec{v}$, T, and also the traceless and symmetric part of the pressure tensor p_{ij}, and the heat flux vector $\vec{q}$. From Grad's method nonlinear transport equations emerge naturally. In connection with generalized hydrodynamics see [5,6]. For a comparison with phenomenological derivations in the case of higher order corrections to the Navier-Stokes equations see [7].

Presently it is possible to get semiexperimental results from microscopic computational simulations using *molecular dynamics* (MD) techniques in which the microscopic interactions are part of the data and they are not bound to being realistic. MD simulations—in the sense of this paper—are a computational technique which traces the microscopic *Newtonian* time evolution of a system of N classical particles in the phase space of all of them.

MD gives extra meaning to another fundamental approach: the linear response Green-Kubo method (GK method from now on) for the calculation of transport coefficients as time integrals of time correlation functions of certain microscopic currents [8]. With the advent of computational physics it became possible to apply the GK method to obtain estimates of the transport coefficients for particular interaction laws. Simulations and these calculations led not only to the conviction that there are long time tails of the GK time correlation functions implying the *divergence of the GK transport coefficients in two dimensions* (2D) but also, for the 3D case, to numerous specific results for self-diffusion, mutual diffusion, bulk and shear viscosity, and thermal conductivity of model gases and liquids, forming an important basis for the dominant interpretation of both the theory and phenomenology of transport.

*Electronic address: drisso@alihven.ciencias.ubiobio.cl
†Electronic address: pcordero@tamarugo.cec.uchile.cl

In particular, the divergence of the 2D transport coefficients has been widely accepted [9]. They are expected to diverge because the corresponding correlation integrals are believed to decay in 2D as $O(1/t)$. On the other hand, recent high precision simulations as in [10–14] for short range steep repulsive potential (hard disks in [14]) produced what looks like size-independent transport coefficients fairly close to the predictions derived from the 2D Enskog theory [15]. No divergence is detected. The reproducible finite nature of viscosity in [10–12] and thermal conductivity in [13,14] could be made understandable if the coefficients give indications of their divergence for systems so large that the limit is beyond present computational possibilities. Certainly the GK derivation of divergence fails to hold for *finite systems* with finite steady state nonequilibrium fluxes. One should find a bridge from finite to infinite systems, a goal that is beyond our present scope.

The Couette flow of a dilute system of Maxwell particles under strong strain has been studied theoretically using the BKG equation [16,17]. In [16] the momentum flux turns out to be a nonanalytic function of the shear rate and the heat current obeys a Fourier law with a conductivity that depends on the shear rate as well. In [17] the authors introduce an external nonconservative force that creates the heat flux. There is no temperature gradient, a drag force is included to preserve the stationary state and it is shown that shear affects the heat flux. The authors present explicit expressions for the shear-dependent thermal conductivity tensor. The off-diagonal terms imply a component of the heat current normal to the temperature gradient as a second order effect not present in the linear constitutive hydrodynamic equations.

We have performed MD simulations of a planar bidimensional Couette flow for a system of hard disks between two flat parallel walls that move with velocities v_0 and $-v_0$, respectively. Particles obey straight Newtonian dynamics and, in particular, the production of heat is only dissipated through the moving walls which are kept at a fixed temperature T_0. Careful local measurements of the hydrodynamic fields show that our system of hard disks does not obey linear transport equations. Because the system heats up at the center of the Couette channel we observe, as expected, a heat flux with a component perpendicular to the walls which accounts for the heat being dissipated through the walls. But we also observe a *longitudinal* heat current, namely, a heat current parallel to the isotherms.

The aim of this paper is to show that there is an approximate nonlinear explicit analytic answer to the problem of momentum and heat transport in the context of a planar Couette flow. This answer is then validated comparing the analytic results with our MD simulations for the gas of hard disks.

What we have done is to apply the hydrodynamic equations that stem from Grad's formalism to solve Boltzmann's equation without making any further approximations. Grad's formalism adds to the standard hydrodynamic balance equations of mass, momentum, and energy, extra balance equations associated to the pressure tensor and the heat current. These extra dynamical equations are nonlinear and take the place of the usual constitutive transport equations. For the planar stationary Couette flow of hard disks we have been able to integrate this set of dynamic equations in a closed form. In particular, we have derived the density, velocity, and temperature fields as well as explicit forms for the pressure tensor field and the heat current.

With all this information we have been able to derive effective shear-dependent analytic expressions for the viscosity and thermal conductivity coefficients. In particular, we show that the observed heat current vector is fairly well described by our analytic results and the pressure tensor shows an excellent agreement between theory and observations. Our simulations were done with our own algorithms as described in [18] and using the precise measurement routines described in [19].

We have already reported simulations of sheared *dense* hard disk fluids in [19,20]. In them too a non-Newtonian and ''non-Fourier'' behavior is observed in the sense, for example, that a heat flux not orthogonal to the isotherms is observed.

In Sec. II the conditions under which the simulations were performed are described in detail. Section III describes Grad's general formalism and next specializes it to the laminar Couette flow under study, getting a set of coupled differential equations for the shear rate, the temperature profile, and the two components of the heat flux. In it we find the solution of these differential equations which show, in particular, nonlinear equations for heat conduction and of viscous flow. In Sec. IV there is a comparison of the previous theory with the observed simulated system.

II. THE SYSTEM AND SIMULATIONAL CONDITIONS

The system of hard disks, of mass m, is inside an $L\times L$ square box. The vertical walls (along the Y direction) are treated as periodic boundaries, the collisions among particles are perfectly elastic, and the collisions with the hard horizontal walls (along the X direction) are such that they impose a temperature T_0 on the fluid as well as a velocity v_0 at the top wall and $-v_0$ at the bottom wall. To do that the velocities of the particles after each hard wall collision are chosen from a velocity distribution $f(\vec{c})\propto\exp\{-(m/2T_0)[(c_x\pm v_0)^2+c_y^2]\}$. Here and in the following temperature is measured in energy units so that Boltzmann's constant is $k_B=1$. The origin is chosen in the middle of the channel so that the coordinate y varies from $-L/2$ to $L/2$.

The control parameters of the simulations were the number of particles, $N=2539$ or $N=7680$, v_0, and the bulk number density $\overline{n}=N/L^2$. The tangential velocity v_0 of the upper and lower walls was in the range $v_0=0.25\sqrt{T_0/m}$ to $128.0\sqrt{T_0/m}$.

In every simulation the system was relaxed for about 20 thermal diffusion times $t_{\rm diff}$ before local time averages of the main momenta of the distribution $(n,\vec{v},T,p_{ij},\vec{q}\,)$ were taken, in some cases for as long as $4000t_{\rm diff}$. The order of magnitude of $t_{\rm diff}$ comes from the energy balance: $t_{\rm diff}\sim L^2/\kappa_0$ where κ_0 is taken to be the ideal gas thermal diffusivity. In one $t_{\rm diff}$ each particle suffers about 100 particle collisions when $N=2539$ and about 300 when $N=7680$.

One has to bear in mind though that, for finite systems such as the present one, there are velocity and temperature jumps which cannot be neglected, implying that the limits of $T(y)$ and $v_x(y)$ as $y\to\pm L/2$ do not give exactly the values externally imposed.

Calling σ the diameter of the disks, the bulk density $\overline{n}=4\rho_A/\pi\sigma^2$ was fixed so that the fraction of area covered by the disks was 1% (area density $\rho_A=0.01$). With this choice the nonideal corrections to the equation of state are less than 2%.

Throughout this paper some quantities will play a particularly important role, among them the free flight time τ, the adimensional shear rate γ, an adimensional measure of the range of the wall effects, $\mathcal{B}$, and a small adimensional parameter γ_0 (the externally imposed adimensional shear) defined in such a way that it would coincide with γ if the strain were small and uniform ($v_0 \sim 0$),

$$\tau(y)=\frac{1}{2\sigma p(y)}\sqrt{\frac{mT(y)}{\pi}}, \tag{1}$$

$$\gamma(y)=\tau(y)v_x'(y), \tag{2}$$

$$\mathcal{B}=\frac{\ell}{L}=\frac{\sqrt{2\pi}}{8\sqrt{\rho_A N}}, \tag{3}$$

$$\gamma_0=\frac{2v_0\ \tau_0}{L}=\frac{4\mathcal{B}}{\sqrt{\pi}}\sqrt{\frac{\frac{1}{2}mv_0^2}{T_0}}, \tag{4}$$

where p is the hydrostatic pressure, ℓ the ideal gas mean free path, $\ell=\pi\sigma/8\sqrt{2}\rho_A$, τ_0 the strain-free mean free flight time, $\tau_0=1/(2\sigma\overline{n})\sqrt{m/(\pi T_0)}$, and the prime indicates derivative with respect to y. Most of our results are presented for situations where $\gamma\approx 0.06$.

The number of disks was chosen so that $\mathcal{B}$ is small enough to keep the boundary effects constrained to a small fraction of the system and guarantee that far from the walls the fluid has a hydrodynamic behavior. For our choice $\rho_A=0.01$, this implies $\mathcal{B}=0.062$, $L=446.6\sigma$ for $N=2539$ and $\mathcal{B}=0.036$, $L=776.7\sigma$ for $N=7680$.

III. BALANCE EQUATIONS AND BOUNDARY CONDITIONS

A. General theoretical framework

For two dimensional dilute gases Grad's distribution is

$$f(\vec{r},\vec{c},t)=\left(1+\frac{1}{nT^2}\left[\left(\frac{mC^2}{4T}-1\right)\vec{C}\cdot\vec{q}+\frac{1}{2}\mathbf{p}:\vec{C}\vec{C}\right]\right)f_0, \tag{5}$$

where $\vec{q}$ is the heat flux vector, $\mathbf{p}$ is the traceless and symmetric part of the pressure tensor, and f_0 is Maxwell's local equilibrium distribution

$$f_0(\vec{r},\vec{c},t)=\frac{nm}{2\pi T}\exp\left[-\frac{mC^2}{2T}\right], \tag{6}$$

$\vec{c}$ is the microscopic velocity, $\vec{v}(\vec{r},t)$ is the hydrodynamic velocity, and $\vec{C}(\vec{r},t)=\vec{c}-\vec{v}(\vec{r},t)$ is the peculiar velocity.

From Boltzmann's equation it is possible to derive balance equations for the momenta of the distribution as a textbook exercise [21]. The first momenta give rise to the standard hydrodynamics equations: the mass, momentum, and energy balance equations. The balance equations associated to the following momenta lead to equations that take the place of the constitutive equations but, strictly speaking, they are dynamic equations for p_{ij} and $\vec{q}$.

We have reconstructed Grad's derivation of these extra approximate equations, for the bidimensional case of a gas of hard disks, obtaining

$$\frac{\partial p_{ij}}{\partial t}+\frac{\partial}{\partial x_k}(v_k p_{ij})+\frac{1}{2}\left(\frac{\partial q_i}{\partial x_j}+\frac{\partial q_j}{\partial x_i}-\delta_{ij}\frac{\partial q_k}{\partial x_k}\right)+p_{rj}\frac{\partial v_i}{\partial x_r}+p_{ri}\frac{\partial v_j}{\partial x_r}-\delta_{ij}p_{rs}\frac{\partial v_s}{\partial x_r}+p\left(\frac{\partial v_i}{\partial x_j}+\frac{\partial v_j}{\partial x_i}-\delta_{ij}\frac{\partial v_r}{\partial x_r}\right)+\frac{1}{\tau}p_{ij}=0 \tag{7}$$

and

$$\frac{\partial q_k}{\partial t}+\frac{\partial}{\partial x_r}(v_r q_k)+\frac{3}{2}\frac{\partial v_k}{\partial x_r}q_r+\frac{1}{2}\frac{\partial v_r}{\partial x_k}q_r+\frac{1}{2}\frac{\partial v_r}{\partial x_r}q_k+\frac{T}{m}\frac{\partial p_{kr}}{\partial x_r}+3p_{kr}\frac{\partial}{\partial x_r}\frac{T}{m}-\frac{p_{kr}}{\rho}\frac{\partial P_{rs}}{\partial x_s}+2p\frac{\partial}{\partial x_k}\frac{T}{m}+\frac{1}{2\tau}q_k=0, \tag{8}$$

where τ was defined in Eq. (1) and p is the hydrostatic pressure. The hydrodynamic equations for the dilute 2D system of hard disks correspond to the standard balance equations plus Eqs. (7) and (8). In the final results it is convenient to replace p_{ij} in favor of the complete pressure tensor $P_{ij}=p_{ij}+p\delta_{ij}$.

As an illustration of their use consider the first equation. Neglecting time variations and all gradients except for the velocity gradient yields

$$p_{ij}=-\eta_0\left(\frac{\partial v_i}{\partial x_j}+\frac{\partial v_j}{\partial x_i}-\frac{\partial v_r}{\partial x_r}\delta_{ij}\right), \tag{9}$$

where the shear viscosity η_0 for hard disks is τp which can be reduced, using Eq. (1), to the standard expression $\eta_0=(1/2\sigma)\sqrt{mT/\pi}$. In a similar fashion one can find, from Eq. (8), the expression for the thermal conductivity $k_0=4\tau p/m$.

B. The laminar flow case

Under conditions of laminar Couette flux and after times much larger than t_{diff} the system is in a stationary regime and the flux presents translation invariance along the Couette channel. All quantities of interest are either uniform or they depend solely on the transversal coordinate y. The hydrodynamic velocity has a unique nonvanishing component $v_x(y)$. The mass balance equation is identically satisfied.

To compare our simulational results with theory the following considerations are made. (i) Grad's solution cannot be expected to be valid near the boundaries ($y=\pm L/2$), where the interaction with the walls plays an important distorting role, particularly at low densities. (ii) Assuming that Grad's solution gives the correct behavior for the system in the bulk, the expressions should reproduce the simulational results using corrected values for v_0 and T_0.

From the momentum balance equation it follows that both P_{xy} and P_{yy} are uniform. Hence, the balance equations (7) for P_{xx} and P_{yy} yield two algebraic relations,

$$p(y)=P_{yy}-\frac{3}{2}\gamma(y)P_{xy}, \quad P_{xx}(y)=P_{yy}-3\gamma(y)P_{xy}, \tag{10}$$

where $\gamma(y)$ is the adimensional shear rate defined in Eq. (1).

The rest of the balance equations yield

$$\frac{\tau}{2}q_x'=-P_{xy}-\gamma P_{yy}, \tag{11}$$

$$q_x+3\gamma q_y=-\frac{6\tau}{m}P_{xy}T', \tag{12}$$

$$\gamma q_x+q_y=-\frac{3\tau}{m}P_{xy}T\gamma'-\frac{\tau}{m}(4P_{yy}+3\gamma P_{xy})\ T', \tag{13}$$

$$\tau q_y'=-\gamma P_{xy}. \tag{14}$$

The primes indicate derivatives with respect to y. The above system of equations has as unknowns the fields γ, T, q_x, q_y. The boundary conditions are

$$T(\pm L/2)=T_0, \quad q_x(0)=0, \quad q_y(0)=0 \tag{15}$$

plus two integral conditions, one that follows simply from $\int n\ dx\ dy=N$ and the second that states that the velocities $\pm v_0$ at the boundaries are known,

$$\int_{-L/2}^{L/2}\frac{p(y)}{T(y)}\,dy=\frac{N}{L} \quad \text{and} \quad \int_{-L/2}^{L/2}\frac{\gamma(y)}{\tau(y)}\,dy=2v_0. \tag{16}$$

The ideal gas equation of state, $p=nT$, was used in the first integral expression while in the last expression the integrand is v_x'.

C. Expansions

At first glance one cannot hope to find a closed analytic solution to the above system of differential equations therefore we expand in terms of γ_0 defined in Eq. (4),

$$\gamma(y)=\gamma_0+\gamma_0^3\eta_3(y)+\gamma_0^5\eta_5(y)+\cdots. \tag{17}$$

There is a symmetry related to inverting the sign of v_0 (or γ or γ_0). It is easy to see that T, q_y, and P_{yy} have to be even in γ_0 while q_x and P_{xy} have to be odd functions of γ_0.

Since q_y vanishes for zero strain its expansion begins with a term $O(\gamma_0^2)$. Similarly, since T' vanishes for zero strain then $T=T_0+O(\gamma_0^2)$. From this and Eq. (12) it follows that q_x is $O(\gamma_0^3)$. Finally since for zero strain the component P_{yy} coincides with the hydrostatic pressure and the pressure is nT then the form $P_{yy}=nT_0+O(\gamma_0^2)$ is used.

With all the above considerations we have solved the system of equations and their boundary conditions in a consistent way using expansions up to γ_0^8. All the algebraic manipulations were done using the symbolic language MAPLE. To our surprise the coefficients η_k that appear in the expansion of γ turn out to be *independent of y* as if the shear rate in the bulk of the system were uniform. The conclusion then is that within the theoretical picture constructed from Grad's 2D eight momentum distribution function (5) (for the bulk of the system) it is reasonable to assume that *the shear rate γ is uniform*. The nonuniformity observed in Fig. 1, when the externally imposed strain is high, may be due to boundary effects and not to a deviation of the theory in the bulk where Grad's distribution should be good.

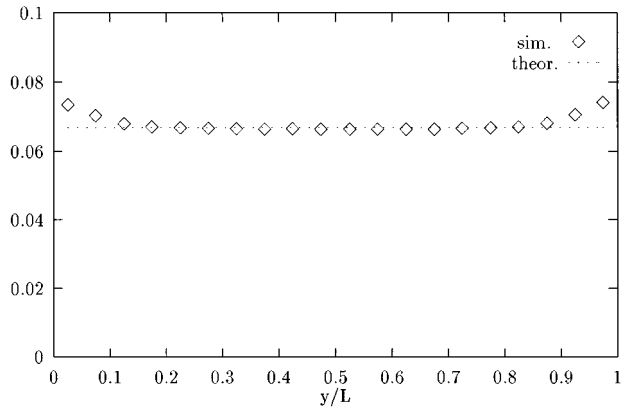

FIG. 1. Profile of the shear rate γ for a system with $N=7680$, $\rho_A=0.01$, and $v_0=1.4\sqrt{T_0/m}$. The horizontal line represents the theoretical value $\gamma=0.066\,869\pm0.000\,062$ explained in the main text. Away from the walls the discrepancy is about 0.9%.

Regarding the last point it is necessary to bear in mind that Grad's approximate solution (5) neglects the contribution from higher momenta which will become important if the shear rate is sufficiently large. The higher balance equations (7) and (8) are implications of Grad's solution where again the contributions from higher momenta are consistently dropped. We have not worked out the necessary formalism to estimate up to which value of the shear rate the present approximation should be expected to be valid.

The Reynolds number $\mathrm{Re}=v_0L/\nu_0$, where ν_0 is the ideal gas kinematic viscosity, reduces in the present case to $8\rho_A N\gamma$ which for the typical values we use amounts to Re up to 20 ($N=2539$) and up to 60 ($N=7680$). However, since for fixed values of v_0 and T_0 the variables γ_0 or γ get smaller for larger systems the higher order corrections would be important only for not too large N but, according to Eq. (17), $\gamma\sim O(1/\sqrt{N})$, implying the Reynolds number increases as $\sqrt{N}$ with N.

D. Closed solution when the shear rate is uniform

First we are going to derive expressions where the coordinate y does not appear explicitly. They are obtained by simple algebraic manipulations of our equations after the term γ' has been erased.

Since γ does not depend on y both Eqs. (12) and (13) have right hand sides proportional to $\tau\ T'$ with constant coefficients. From Eq. (12) follows an expression for T' which is replaced in Eq. (13) to get an expression for q_x proportional to q_y. This q_x is used in Eq. (11) to get an expression for $q_y{}^*$ which is equated to the expression for q_y' in Eq. (14). The result is an algebraic expression for P_{xy}/P_{yy} and if this P_{xy} is replaced back in the expression for q_x an expression for the ratio between the two components of the heat

current follows. The two ratios turn out to be

$$\frac{P_{xy}}{P_{yy}}=\frac{4+3\gamma^2-\sqrt{\Delta}}{3\,(4-3\gamma^2)\,\gamma}\approx-\gamma+\frac{9}{4}\,\gamma^3+\cdots, \tag{18}$$

$$\frac{q_x}{\gamma q_y}=-\frac{18\,(2-\gamma^2)}{4-3\gamma^2+\sqrt{\Delta}}\approx-\frac{9}{2}+9\gamma^2-\frac{135}{4}\,\gamma^4+\cdots, \tag{19}$$

where $\Delta=16+120\gamma^2-63\gamma^4$. Observe that Eq. (19) implies that there is a heat flux current q_x *along* the Couette channel. For shears as small as $\gamma=0.065$ Eq. (19) predicts a heat current which can be as large as 30% the size of the transversal heat current q_y, as indeed is observed in our simulations described in the next section.

(a) Shear viscosity. From the expression for P_{xy}/P_{yy} and $p=P_{yy}-\frac{3}{2}\gamma P_{xy}$ it is direct to obtain that the shear viscosity $\eta\equiv-P_{xy}/v_x'$ is

$$\frac{\eta}{\eta_0}=\frac{8}{15\gamma^2+4+\sqrt{\Delta}}\approx1-\frac{15}{4}\,\gamma^2+\frac{297}{16}\,\gamma^4+\cdots, \tag{20}$$

where η_0 was already defined below Eq. (9). The expression above predicts an effective shear thinning which is compared with our observations in Fig. 4. The agreement is excellent as we show in the next section.

(b) Thermal conductivity tensor. Once the term with γ' was eliminated from Eq. (13), the use of that equation and Eq. (12) directly leads to expressions

$$q_y=-k_{yy}\,T' \quad \text{and} \quad q_x=-k_{xy}\,T', \tag{21}$$

with

$$k_{yy}=\frac{1-\frac{3}{4}\,\gamma P_{xy}/P_{yy}}{1-3\gamma^2}\,k_0$$

and

$$k_{xy}=\frac{-3\gamma+(3P_{xy}/2P_{yy})\left(1-\frac{3}{2}\,\gamma^2\right)}{1-3\gamma^2}\,k_0 \tag{22}$$

but since the ratio P_{xy}/P_{yy} was already determined in Eq. (18) it follows that

$$\frac{k_{yy}}{k_0}=\frac{8}{4-33\gamma^2+\sqrt{\Delta}}\approx1+\frac{9}{4}\,\gamma^2+\frac{153}{16}\,\gamma^4+\cdots, \tag{23}$$

$$\frac{k_{xy}}{k_0}=\frac{9\gamma^4-6\gamma^2+8+(9\gamma^2-2)\sqrt{\Delta}}{48\gamma^2(1-3\gamma^2)}\approx-\frac{9}{2}\,\gamma-\frac{9}{8}\,\gamma^3+\cdots. \tag{24}$$

In the above results there appears no explicit dependence on the coordinate y. Notice, however, that η_0 and k_0 are proportional to $\sqrt{T(y)}$. The problem of determining the transport coefficients themselves has been reduced to determining η_0 and k_0 and therefore to determining the temperature profile.

(c) The temperature profile. If we go back to the original equations and notice that τ depends on y only through $\sqrt{T}$ then Eqs. (12) and (13) imply that both heat currents q_k are proportional to $(T^{3/2})'$. Hence both Eqs. (11) and (14) imply that $\sqrt{T}(T^{3/2})''$ is a constant and an expression for the temperature profile is easily obtained.

$$TT''+\frac{1}{2}T'^2+K=0, \tag{25}$$

which can be integrated for y in terms of T,

$$\pm\sqrt{2K}\;y=T\;\sqrt{\frac{T_{\max}-T}{T}}+T_{\max}\arctan\sqrt{\frac{T_{\max}-T}{T}}, \tag{26}$$

where

$$\sqrt{2K}=\frac{\sqrt{81\gamma^4-264\gamma^2+16+(15\gamma^2+4)\;\sqrt{\Delta}}}{4-3\gamma^2}\sqrt{\pi}\sigma\gamma P_{yy}$$

$$\approx\left(\gamma-\frac{3}{2}\,\gamma^3-\frac{9}{8}\,\gamma^5-\frac{27}{32}\,\gamma^7+\cdots\right)\;\sqrt{2\pi}\sigma P_{yy}. \tag{27}$$

$\sqrt{2K}$ is real in the interval $0<\gamma^2<\frac{1}{3}$. The $\pm$ on the left hand side of Eq. (26) is natural because the symmetry of the system implies that under laminar conditions the temperatures at y and $-y$ are the same. In practice to integrate Eq. (25) we imposed that at the center of the channel $T(0)=T_{\max}$ and $(dT/dy)_{y=0}=0$ even though we do not know yet the value of $T_{\max}$. In Fig. 2 there is a comparison of the observed values of T' and the corresponding profiles obtained from the above expressions. Comments are deferred to Sec. IV.

What remains now is to connect the uniform fields P_{yy}, $T_{\max}$, and γ with the control parameters v_0 and T_0 (or rather to adimensional parameters γ_0 and $\mathcal{B}$) and the parameters of the system $(\rho_A,\sigma,L,N,\ldots)$.

(d) Using the integral boundary conditions. From the knowledge of $T(y)$ it is quite easy to actually make the integrals that appear in the integral boundary conditions, for example, $\int dy/T=4/\sqrt{2K}\,\arctan\sqrt{(T_{\max}-T_0)/T_0}$.

The two integral boundary conditions (16) combined render

$$\sqrt{\frac{T_{\max}-T_0}{T_0}}=\frac{\sqrt{\pi}}{4}\,\frac{\gamma_0}{\mathcal{B}}\sqrt{\frac{1-3\gamma^2}{4+9\gamma^2+\sqrt{\Delta}}}$$

$$=\frac{\gamma_0}{\mathcal{B}}\,\frac{\sqrt{\pi}}{8}\left(1-3\gamma^2+\frac{27}{4}\,\gamma^4+\cdots\right) \tag{28}$$

and

$$\sqrt{\frac{T_{\max}-T_0}{T_0}}=\frac{\gamma_0}{\gamma}\,\arctan\sqrt{\frac{T_{\max}-T_0}{T_0}}. \tag{29}$$

Using Eq. (28) on both sides of Eq. (29) one has γ as a function of the external parameters γ_0 and $\mathcal{B}$. Fixing $\mathcal{B}$ one can plot γ as a function of γ_0. Once this is done Eq. (28) gives $T_{\max}$ in terms of T_0, γ_0, and $\mathcal{B}$. Since the previous equations are implicit such plots have to be constructed using numerical methods.

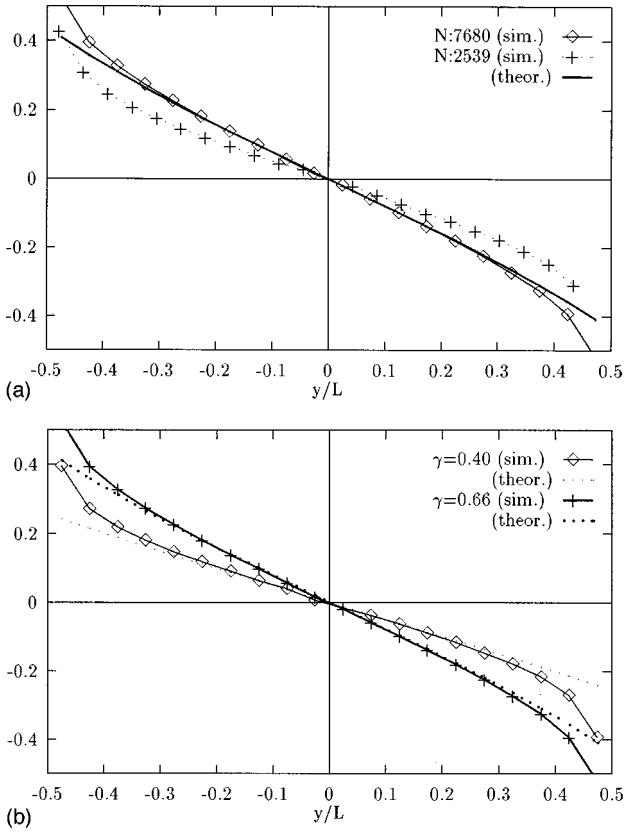

FIG. 2. At top $T'(y)$ for two systems with $\rho_A=0.01$: $N=2539$, $\gamma=-0.063$, and $N=7680$, $\gamma=-0.058$. The theoretical profile T' for both cases are indistinguishable in this figure. The smaller system clearly differs from the theoretical profile. At bottom two profiles $T'(y)$ for $N=7680$ but different γ. Away from the walls theory and observations coincide. The temperature gradient is scaled with the square root of $2K$.

When $\frac{1}{2}mv_0^2 \ll T_0$ $(\gamma \to 0)$ Eq. (28) leads to $\sqrt{(T_{\max}-T_0)/T_0} \approx \sqrt{\pi}\gamma_0/(8\mathcal{B})$. On the other hand, the large shear limit cannot be reliable since in the present approach it is being assumed that the shear rate is not too large. Still, this limit corresponds to neglecting T_0 in front of $T_{\max}$ and Eq. (28) leads to $T_{\max} \approx \frac{1}{2}mv_0^2$ and $\gamma \to \gamma_\infty \equiv (\pi/4)(1/\sqrt{2N\rho_A})$ suggesting that—for a given system (N fixed)—γ does not grow indefinitely. Qualitatively our simulational results suggest that γ saturates, see Table I. Understandably though, the observed asymptotic value that γ seems to have is not close to the previous γ_∞.

From the condition $T(\pm L/2)=T_0$ follows an expression for P_{yy} which can be reduced to

$$P_{yy}=\frac{NT_0}{L^2}\,\frac{4-3\gamma^2}{4-9\gamma^2+\sqrt{\Delta}}\left(1+\frac{\gamma_0}{\gamma}+\frac{T_{\max}-T_0}{T_0}\right). \quad (30)$$

The expression for $(T_{\max}-T_0)/T_0$ given in Eq. (28) can be replaced in Eq. (30) to have an explicit expression for P_{yy} in terms of the shear rate γ. In the small shear rate limit the last bracket tends to 2 and the middle fraction tends to $\frac{1}{2}$, making P_{yy} tend to the hydrostatic pressure $p=nT_0$ as it should. This expression of P_{yy} in terms of γ can be replaced back in Eq. (27) and get an expression for $\sqrt{2K}$.

IV. OBSERVATIONS VERSUS THEORY

A. Generalities and boundary effects

To measure the hydrodynamic behavior of the system, the box was divided in $M_x \times M_y$ rectangular cells. In each cell the time average of the first momenta of the distribution was made. For the system with $N=7680$ particles the choice was $M_x=M_y=20$, which corresponds to about 19.2 disks per cell and in the case with $N=2539$ it was $M_x=M_y=23$ or about 4.8 disks per cell. Units are chosen so that the mass of each particle is $m=1$, their diameter is $\sigma=1$ and time units such that the temperature T_0 at the horizontal walls, measured in energy units ($k_B=1$), is fixed to be $T_0=1$.

To measure the number density n, the hydrodynamic velocity $\vec{v}$, and the temperature T the algorithm carries in each cell an exact integration over time of the number of disks, total momentum, and total kinetic energy (*densities*). To

TABLE I. Simulational values of P_{xy}, P_{yy}, and γ versus the imposed tangential velocity v_0. In the third column are the values of the shear rate obtained from Eq. (18). The averages for the uniform quantities were taken in the whole volume of the system. The *simulational* value of γ is an average over four values measured at the central part of the fluid. The numbers in square brackets denote powers of 10.

$\frac{v_0}{\sqrt{T_0/m}}$	γ sim.	γ theor.	$\frac{P_{xy}}{T_0/\sigma^2}$	$\frac{P_{yy}}{T_0/\sigma^2}$
0.2	0.010285	0.010370	0.000140±7[-11]	0.013511±6[−8]
0.8	0.040127	0.040437	0.000580±4[−6]	0.014399±6[−8]
1.0	0.049442	0.049547	0.000735±4[−6]	0.149180±1[−11]
1.4	0.066253	0.066869	0.001079±1[−6]	0.016297±1[−7]
2.0	0.087807	0.088711	0.001668±4[−6]	0.019129±5[−7]
8.0	0.166661	0.169997	0.014237±2[−5]	0.088909±1[−7]
16.0	0.184631	0.189379	0.050967±3[−5]	0.289465±1[−6]
32.0	0.192817	0.198525	0.193722±2[−4]	1.056361±2[−6]
56.0	0.195729	0.202106	0.578589±6[−1]	3.107144±4[−5]
128.0	0.199432	0.205384	2.966890±5[−3]	15.71608±2[−4]
256.0	0.201661	0.207323	11.69858±2[−2]	61.47708±3[−4]

measure *currents*, namely, the pressure tensor P_{ij} and the heat current $\vec{q}$, it is necessary to measure separately the kinetic and the collisional contributions. The kinetic contributions come from the fluxes using the peculiar velocity $\vec{C}$, namely, the fluxes mC_iC_j and $\frac{1}{2}mC^2C_k$ that take place each time a disk enters or leaves a cell. Regarding the collisional contributions we estimate, using Gass's expressions for the transport coefficients [15] for hard disks (linear constitutive equations) that they will be of the order of 2%.

Most quantities show boundary effects. The temperature field shows isotherms parallel to the flow but—as predicted by Eq. (19)—the heat flux is not orthogonal to them: it bends in the direction of the mass flow. The equation of state is well satisfied across the fluid, including the regions near the walls. Observed discrepancies with the ideal gas equation were always below 2% and if Henderson's equation of state [22] is used the discrepancies are below 0.1% for the $N=7680$ system. The components P_{xy} and P_{yy} of the pressure tensor show no boundary effects but P_{xx} does.

Taking advantage of the translation invariance in the X direction, it was natural to take horizontal averages of the observed cell results getting in this way smooth vertical profiles for the observed hydrodynamic fields.

As mentioned above Eq. (10), P_{xy} and P_{yy} should be uniform and this is what we in fact observe. From the horizontal averages of P_{xy} and P_{yy}, for $N=2539$ particles, their values at each y are obtained with errors of less than 0.6% and less than 0.07%, respectively. For the larger system the errors are still smaller. An additional vertical average over each of the previous profiles produce a variance of about 0.1% for P_{xy} and of about 0.008% for P_{yy} when $N=2539$ and smaller when $N=7680$. In this sense it can be stated that these two quantities are independent of y as hydrodynamics predicts. In Table I we have summarized our results for the system with $N=7680$ and $\rho_A=0.01$.

Even though we derived that up to eighth order in γ_0 the adimensional shear rate γ is uniform, the simulations for shear rates as small as $\gamma\sim 0.06$ show a wide region near the boundaries of the channel where γ [evaluated through Eqs. (1), (2), and $p=\frac{1}{2}\mathrm{Tr}\mathbf{P}$] noticeably varies with y. In the central region γ is quite uniform as seen in Fig. 1.

From these considerations it is clear that the theoretical framework presented in Sec. III needs a reassessment because, even though the differential equations are expected to be valid in the bulk, this is not true near the boundaries. The closed expressions found in Sec. III D should be expected to fit well away from the walls and the values associated to the boundary conditions (T_0,v_0) should be adjusted to make this fit.

B. Results fits

To adjust the observed results we proceeded as follows.

The shear rate γ. Since both P_{xy} and P_{yy} are independent of the coordinate y within a very small error, vertical averages of these two quantities were taken and from them and Eq. (18) an effective value for the shear rate γ is obtained. The fourth and fifth columns of Table I show the measured values of P_{xy}, P_{yy}. In the second column is the value of γ evaluated using Eq. (1) for the four values measured at the center of the channel while in the third column is the effective theoretical value of γ. For $v_0<8\sqrt{T_0/m}$ the discrepancies are less than 1%.

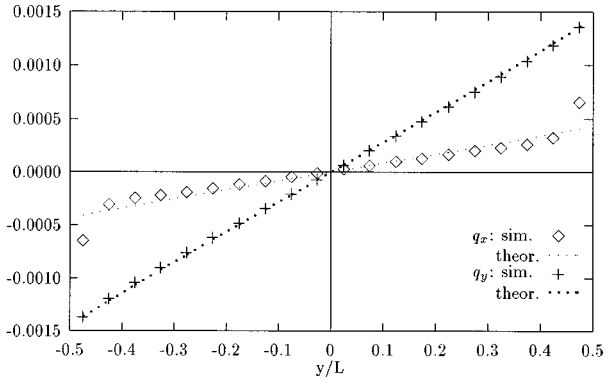

FIG. 3. The theoretical and observed profiles of the heat currents $\vec{q}$ for a system of $N=7680$. The theoretical γ is $\gamma=0.066\,869\pm0.000\,062$. The transversal heat current q_y (with crosses) shows excellent agreement with the theory, while the agreement between the theoretical and observed profiles of the longitudinal heat current q_x (with rhombus) is fair. Both currents are scaled with the factor $T_0\sqrt{T_0/m}$.

Figure 1 shows the adjusted γ and the observed shear rate profile. The figure corresponds to the case $N=7680$ and $v_0=1.4\sqrt{T_0/m}$. Away from the walls the adjusted value of γ is $\gamma=0.066\,869\pm0.000\,062$ which differs from the observed value in about 0.9%. Similar differences are obtained for other values of v_0. In the extreme case $v_0=128\sqrt{T_0/m}$ the γ profile is less uniform and the values in the central part of the box and border differ by about 4% and the difference between the simulational value of γ in the central zone and the theoretical value reaches a 3%.

The constant $\sqrt{2K}$ is evaluated from Eq. (27).

The temperature $T_{\max}$ *and* $T(y)$. $T_{\max}$ was obtained making a mean square fit of Eq. (26) adjusting both the values of $T_{\max}$ and again the value of $\sqrt{2K}$. Since the temperature profile shows a strong and wide boundary effect different fits were made eliminating one, two, three, etc. points on each extreme and finally an extrapolation was made. The value for $\sqrt{2K}$ obtained in this way differs from the one obtained from Eq. (27) by a few percent.

The previous fit yields what we will be calling the theoretical temperature profile $T(y)$ from now on. It coincides with the observed T profile only in the central region and fails badly away from it. From the theoretical temperature profile $T(y)$ follows its gradient $T'(y)$. In Fig. 2 there is a comparison of the latter with the observed values. The T' profile agrees quite well away from the walls when the system is larger ($N=7680$).

The heat currents q_y *and* q_x. Figure 3 compares the observed heat flux profiles with the theoretical profiles given in Eq. (21) for the case $N=7680$, $\gamma\approx0.067$. Crosses indicate the simulational values of the transversal heat current q_y. Notice that q_y, as seen in Eq. (21), obeys a Fourier type of law with an effective conductivity that depends on the shear rate. The agreement with the predicted values of q_y is excellent. Rhombuses are used to show the component of the heat flux current q_x along the isotherms. It is seen that, in the last

TABLE II. Simulational viscosity η/η_0 and conductivities k_{xy}/k_0, k_{yy}/k_0 versus the simulational γ for the $N=7680$ system.

$\frac{v_0}{\sqrt{T_0/m}}$	γ sim.	η/η_0	k_{xy}/k_0	k_{yy}/k_0
0.2	0.010285	1.012652	-0.0318 ± 0.014	
0.8	0.040127	1.001918	-0.1557 ± 0.007	0.9550 ± 0.007
1.0	0.049442	0.993623	-0.1982 ± 0.020	1.1190 ± 0.040
1.4	0.066253	0.993362	-0.2699 ± 0.006	1.0210 ± 0.015
2.0	0.087807	0.981536	-0.3459 ± 0.014	1.0560 ± 0.040
8.0	0.166661	0.924016	-0.5360 ± 0.006	0.8534 ± 0.005
16.0	0.184631	0.910397	-0.5599 ± 0.003	0.8166 ± 0.006
32.0	0.192817	0.905053	-0.5734 ± 0.002	0.7995 ± 0.005
56.0	0.195729	0.903687	-0.6248 ± 0.027	0.8569 ± 0.046
128.0	0.199432	0.898152	-0.5790 ± 0.010	0.7887 ± 0.008
256.0	0.201661	0.894963	-0.5782 ± 0.008	0.7857 ± 0.004

case, the agreement is fair. For $N=2359$ the q_x fit is rather poor (the boundary effects propagate deeper into the system) and we did not make the corresponding plot. In general the boundary effects for a fixed γ are seen to be smaller for larger systems as the definition (3) of $\mathcal{B}$ suggests.

The integral boundary conditions. To check the implications of the integral boundary conditions we proceeded to determine the value of γ that follows from Eqs. (28) and (29). Taking the system with $N=7680$, $v_0=1.0\sqrt{T_0/m}$ and using for T_0 the value obtained from the theoretical profile, we obtain $\gamma=0.049\,537\,8$ while the value of γ derived from P_{xy}/P_{yy} is $\gamma=0.049\,546\,8$ which is better than what one could expect.

In the case of small γ, the expression (28) predicts via Eqs. (3) and (4) a temperature difference $T_{\max}-T_0 \approx(\pi/64)T_0(\gamma_0/\mathcal{B})^2$, implying that, because $\mathcal{B}$ is small, there is a significant heating of the central part of the channel. In particular, for the case $\gamma\sim0.049\,54$ (which corresponds to $v_0=1.4\sqrt{T_0/m}$) Eq. (28) predicts $(T_{\max}-T_0)/T_0\approx0.125$ while we observe 0.2 and for $\gamma\sim0.066\,25$ (which corresponds to $v_0=1.0\sqrt{T_0/m}$) Eq. (28) predicts 0.245 while we observe 0.29. The discrepancies may be due to boundary effects.

The shear viscosity. Using the observed values of v_x' and P_{xy} at different points in the channel and in different simulations it is possible to extract a simulational value for the shear viscosity ratio η/η_0 (see Table II) which turns out to follow quite well the value given in Eq. (20) within less than 1% in a range of γ up to $\gamma=0.2$ (see Fig. 4). We have not enough data to derive error bars but all points are seen to fall close to the theoretical curve.

The thermal conductivity coefficients. Similarly, the observed components of the thermal conductivity tensor are compared with the expression implied by Eqs. (23) and (24). From the observed values for q_x, q_y, and T' we have derived profiles for the conductivities $k_{xy}=-q_x/T'$, $k_{yy}=-q_y/T'$ after eliminating two or three data points from the borders and four noisy points from the central part where T',q_x,q_y are too small. An extrapolation of the profiles of k_{xy}/k_0 and k_{yy}/k_0 at $y=0$ using a parabolic fit yields the simulational values presented in Table II for different values of the simulational γ.

For k_{xy}/k_0 the agreement is quite good if $v_0\leqslant2\sqrt{T_0/m}$ ($\gamma\leqslant0.087\,807$) when $N=7680$ (see Fig. 5). For k_{yy}/k_0 (see Fig. 6) the statistics are rather poor. The results show a behavior consistent with the theory for small values of the

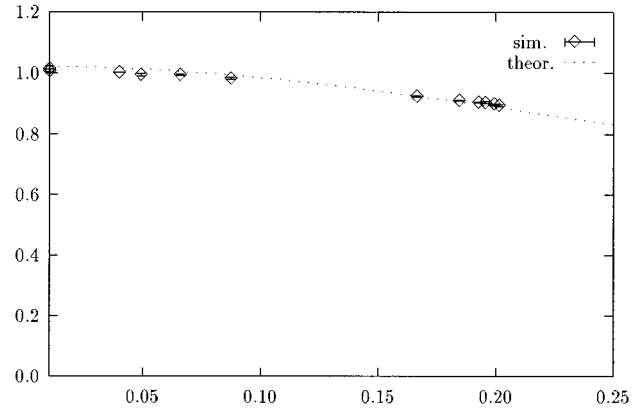

FIG. 4. The predicted viscosity ratio η/η_0, versus γ showing shear thinning, is compared with the viscosity ratio derived directly from the observations ($N=7680$).

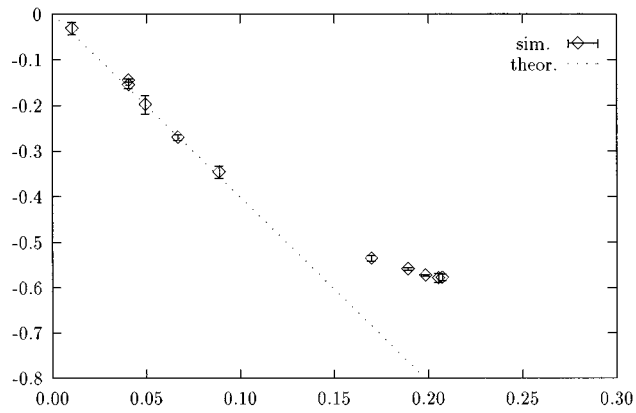

FIG. 5. The predicted k_{xy}/k_0 conductivity ratio versus γ is compared with the conductivity ratio derived directly from the observations ($N=7680$).

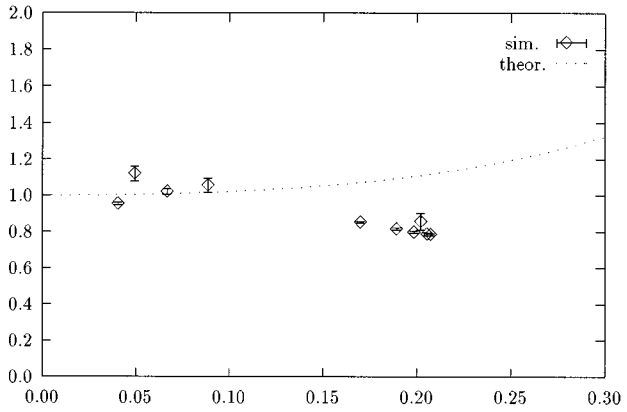

FIG. 6. The predicted k_{yy}/k_0 conductivity ratio versus γ is compared with the conductivity ratio derived directly from the observations ($N=7680$).

shear rate, but we do not have enough data to make stronger statements.

Our data are less noisy when the shear rate gets larger ($v_0 > 2.0\sqrt{T_0/m}$) but in that case the discrepancy with theory is substantial both for k_{xy} and k_{yy}. There are many possible sources for these discrepancies. The higher balance equations (7) and (8) are derived, according to Grad, neglecting terms that involve still higher momenta which possibly are no longer negligible at such high shear rates. The boundary effects, on the other hand, are also more complex since the discontinuities of the hydrodynamic fields at the walls are related to their own gradients. This seems particularly relevant in the case of the temperature field.

In summary, we have used Grad's momentum to derive, from Boltzmann's equation, a hydrodynamics for the gas of hard particles. This hydrodynamics comprises the standard hydrodynamic equations plus dynamic equations for the pressure tensor and the heat current. Hence the only constitutive equation is the equation of state. When applying these equations to the case of a planar Couette laminar flow we find a closed solution which includes the description of nontrivial temperature profile, heat flow both orthogonal to and along the isotherms. The solution is in general an excellent description of what is actually seen, away from the walls, in our molecular dynamics simulations with systems of less than 10^4 particles subjected to extreme shear conditions. In particular, we have found closed analytic expressions for the effective nonlinear transport coefficients for this planar Couette flow.

ACKNOWLEDGMENTS

We thank C. González R. for his valuable help, L. Letamendia for his hospitality at U. de Bordeaux I, and W. Ellison for his help in the use of the Cray belonging to the laboratory Physique des Interactions Ondes Matiere, E.N.S.C.P.B, U. de Bordeaux I. This work was supported by the Fundación Andes Grant No. C-12971 and a CNRS-Conicyt grant. One of us (D.R.) is also thankful for the UBB Diprode research Grant Nos. 951005-2 and 960105-2.

APPENDIX: SOLUTION IN THREE DIMENSIONS

We have been able to find a closed analytic solution in 3D quite similar to the one we have presented for the bidimensional case, only that we do not have simulations to compare with. We have chosen hard walls parallel to the XY plane moving with velocities $\pm v_0$ in the X direction. The only coordinate that plays an interesting role is the z. From the balance equations and symmetry of the problem we have derived that $q_y=0$, $P_{xy}=0$, $P_{yz}=0$ while P_{xz} and P_{zz} are uniform. Again we are able to see that Grad's solution yields a uniform shear rate.

The shear viscosity normalized to the ideal gas case turns out to be

$$\frac{\eta}{\eta_0} = -\frac{2}{1+\frac{12}{25}\gamma^2+\frac{1}{5}\sqrt{\Delta_3}} = 1-\frac{72}{25}\gamma^2+\frac{1356}{125}\gamma^4+\cdots, \tag{A1}$$

where $\Delta_3 = 25+144\gamma^2-48\gamma^4$.

The thermal conductivity coefficients can be expressed in terms of the ratio

$$\frac{P_{xz}}{P_{zz}} = -\frac{2\gamma}{1+\frac{12}{25}\gamma^2+\frac{1}{5}\sqrt{\Delta_3}} \tag{A2}$$

$$= -\gamma+\frac{42}{25}\gamma^3-\frac{672}{125}\gamma^5+\cdots \tag{A3}$$

and they are

$$\frac{k_{zz}}{k_0} = \frac{1-(16\gamma/25)(P_{xz}/P_{zz})}{1-\frac{56}{25}\gamma^2}$$

$$= 1+\frac{72}{25}\gamma^2+\frac{672}{125}\gamma^4+\cdots, \tag{A4}$$

$$\frac{k_{xz}}{k_0} = \frac{7}{5}\frac{-2\gamma+\left(1-\frac{24}{25}\gamma^2\right)(P_{xz}/P_{zz})}{1-\frac{56}{25}\gamma^2}$$

$$= -\frac{21}{5}\gamma-\frac{714}{125}\gamma^3-\frac{14\,412}{628}\gamma^5\cdots. \tag{A5}$$

The temperature profile again satisfies the same equation (25) as in the bidimensional case and therefore has the same

formal solution (26), the difference being in the form of the constant that we now call K_3,

$$\sqrt{2K_3}=\frac{8}{5}\sqrt{\frac{10\pi}{7}}\,\frac{1+\frac{72}{25}\gamma^2+\frac{1}{5}\sqrt{\Delta_3}}{1+\frac{12}{25}\gamma^2+\frac{1}{5}\sqrt{\Delta_3}} \times \sqrt{-1-\frac{44}{25}\gamma^2+\frac{1}{5}\sqrt{\Delta_3}}\;\sigma^2 P_{zz}. \tag{A6}$$

One of the integral boundary conditions is again Eq. (29) while the other takes the form

$$\sqrt{\frac{T_{\max}-T_0}{T_0}}=\frac{\gamma_0}{\mathcal{B}}\,\frac{4}{5\sqrt{10\pi}}\,\frac{1}{\sqrt{1+\frac{44}{25}\gamma^2+\frac{1}{5}\Delta_3}} \tag{A7}$$

$$=\frac{2\gamma_0\sqrt{5}}{25\mathcal{B}\sqrt{\pi}}\left(1-\frac{29}{25}\gamma^2+\frac{4119}{1250}\gamma^4+\cdots\right). \tag{A8}$$

[1] J. H. Ferziger and H.G. Kaper, *Mathematical Theory of Transport Processes in Gases* (North-Holland, Amsterdam, 1972).

[2] J. O. Hirschfelder, C. F. Curtis, and R. B. Bird, *Molecular Theory of Gases and Liquids* (Wiley, New York, 1954).

[3] P. L. Bhatnagar, E. P. Groos, and M. Krook, Phys. Rev. **94**, 593 (1954).

[4] H. Grad, in *Principle of the Kinetic Theory of Gases*, edited by S. Flügge, Handbuch der Physik Vol. XII (Springer, Berlin, 1958).

[5] J. P. Boon and S. Yip, *Molecular Hydrodynamics* (Dover Publications, New York, 1980).

[6] R. M. Velasco and L. S. García-Colín, Phys. Rev. A **44**, 4961 (1991).

[7] L. S. García-Colín, Physica A **118**, 341 (1983).

[8] M. S. Green, J. Chem. Phys. **20**, 1281 (1952); **22**, 398 (1953); R. Kubo, J. Phys. Soc. Jpn. **12**, 570 (1957); H. Mori, Phys. Rev. **112**, 829 (1958); **115**, 298 (1959).

[9] M. H. Ernst, B. Cichocki, J. R. Dorfman, J. Sharma, and H. van Beijern, J. Stat. Phys. **18**, 237 (1978).

[10] W. G. Hoover and H. A. Posch, Phys. Rev. E **51**, 273 (1995).

[11] H. A. Posch, W. G. Hoover, and O. Kum, Phys. Rev. E **52**, 1711 (1995).

[12] D. Gravina, G. Ciccotti, and B. L. Holian, Phys. Rev. E **52**, 6123 (1995).

[13] D. P. Hansen and D. J. Evans, Mol. Simul. **14**, 409 (1995).

[14] D. Risso and P. Cordero, J. Stat. Phys. **82**, 1453 (1996).

[15] D. M. Gass, J. Chem. Phys. **54**, 1898 (1971).

[16] J. J. Brey and Andrés Santos, Phys. Rev. A **36**, 2842 (1987); Ch. S. Kim, J. W. Dufty, A. Santos, and J. J. Brey, *ibid.* **40**, 7165 (1989).

[17] V. Garzó, J. Chem. Phys. **101**, 1423 (1994); Phys. Rev. E **51**, 3156 (1995); J. Chem. Phys. **103**, 4626 (1995).

[18] M. Marín, D. Risso, and P. Cordero, J. Comput. Phys. **109**, 306 (1993).

[19] D. Risso, Ph.D. thesis, Universidad de Chile, 1994.

[20] D. Risso and P. Cordero, in *Instabilities and Nonequilibrium Structures V*, edited by E. Tirapegui and W. Zeller (Kluwer Academic Publishers, Dordrecht, 1996).

[21] D. A. McQuarrie, *Statistical Mechanics* (Harper Collins Publishers, New York, 1976).

[22] D. Henderson, Mol. Phys. **30**, 971 (1975); J. A. Barker and D. Henderson, Rev. Mod. Phys. **48**, 587 (1976).